JCTC Journal of Chemical Theory and Computation

Article

pubs.acs.org/JCTC

Modeling Solvent Broadening on the Vibronic Spectra of a Series of Coumarin Dyes. From Implicit to Explicit Solvent Models

Javier Cerezo,[†] Francisco J. Avila Ferrer,[†,‡] Giacomo Prampolini,[†] and Fabrizio Santoro*[,†]

[†]Istituto di Chimica dei Composti OrganoMetallici, Consiglio Nazionale delle Richerche (ICCOM-CNR), Area della Ricerca, via G. Moruzzi 1, I-56124 Pisa, Italy

[‡]Physical Chemistry, Faculty of Science, University of Málaga, Málaga 29071, Spain

Supporting Information

ABSTRACT: We present a protocol to estimate the solvent-induced broadening of electronic spectra based on a model that explicitly takes into account the environment embedding the solute. Starting from a classical approximation of the solvent contribution to the spectrum, the broadening arises from the spread of the excitation energies due to the fluctuation of the solvent coordinates, and it is represented as a Gaussian line shape that convolutes the vibronic spectrum of the solute. The latter is computed in harmonic approximation at room temperature with a time-dependent approach. The proposed protocol for the computation of spectral broadening exploits molecular dynamics (MD) simulations performed on the solute−solvent system, keeping the solute degrees of freedom frozen, followed by the computation of the excitation properties with a quantum mechanics/molecular mechanics (QM/MM) approach. The factors that might influence each step of the protocol are analyzed in detail, including the selection of the empirical force field (FF) adopted in the MD simulations and the QM/MM partition of the system to compute the excitation energies. The procedure is applied to a family of coumarin dyes, and the results are compared with experiments and with the predictions of a very recent work (Cerezo et al., *Phys. Chem. Chem. Phys.* **2015**, *17*, 11401−11411), where an implicit model was adopted for the solvent. The final spectra of the considered coumarins were obtained without including *ad hoc* phenomenological parameters and indicate that the broadenings computed with explicit and implicit models both follow the experimental trend, increasing as the polarity change from the initial to the final state increases. More in detail, the implicit model provides larger estimations of the broadening that are closer to the experimental evidence, while explicit models appear to better capture relative differences arising from different solvents or different solutes. Possible inaccuracies of the adopted FF that may lead to the observed underestimation are analyzed in detail.

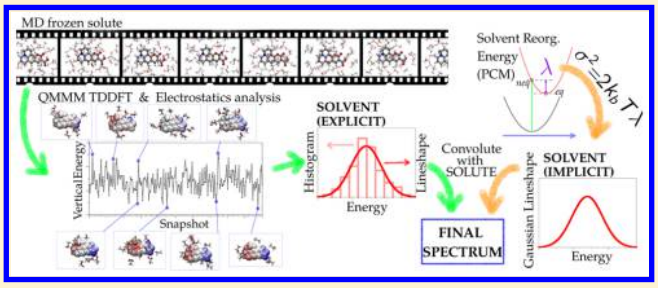

1. INTRODUCTION

UV−vis electronic spectroscopy is a powerful technique with widespread applications in different research fields, ranging from material science to photobiology, since it allows researchers to investigate excited molecular electronic states and their interaction with the environment. Thanks to continuous progresses, computational methods have reached a sufficient maturity to help the interpretation of experimental spectra. In particular, the calculation of low-/intermediate-resolution spectra of semi-rigid molecules in the gas phase or apolar solvents is now rather standard if the electronic states are not involved in strong non-adiabatic interactions, by exploiting either time-independent (TI)[1−7] or time-dependent (TD)[8−16] quantum approaches. The current computational challenges are represented by flexible systems, and solutes in solvents with high polarity or capable of establishing specific interactions with the solute.

The most straightforward route to treat these cases is provided by molecular dynamics (MD) simulations of the solute in explicit solvents. Along these lines, the spectrum is obtained by application of the classical Franck−Condon (FC) principle, i.e. from the distribution of the transition energies computed at the quantum mechanics/molecular mechanics (QM/MM) level of theory of a representative set of snapshots extracted from the MD trajectories (see, for example, refs 17−27).

The main shortcoming of these approaches is that they neglect quantum effects due to solute vibrations. Indeed, theoretical arguments based on the analysis of spectral moments,[28] as well as numerical experiments performed on systems where quantum calculations are feasible, indicate that classical approximations both underestimate the width of the signal and do not reproduce the asymmetry of the spectra.[23] Moreover, in the case of weak transitions, application of the classical FC principle is unable to fully capture the impact of quantum Herzberg−Teller (HT) effects.[28,29] There is no reason to think that these issues should not play a role also for systems in the condensed phase. Clearly, it is possible that in such environment they might be overtaken by the effective

Received: September 10, 2015
Published: November 9, 2015

DOI: 10.1021/acs.jctc.5b00870
J. Chem. Theory Comput. 2015, 11, 5810−5825

spectral broadening, due to solute conformational flexibility and/or fluctuation within the embedding environment. However, only a systematic analysis of the detailed balance among all these effects can unravel the role of each contribution. It should be added that only a method capable of accounting for the quantum features of the solute spectrum can tackle the description of the smooth transition from resolved spectra in apolar solvents to structureless bands in a polar environment, providing a unitary theoretical counterpart to detailed experimental analyses.[30,31]

Quantum methods to compute spectra have actually been generalized to account for some solvent effects. In fact, the adoption of implicit models, like the polarizable continuum model (PCM),[32] allows for the description of mean-field solvent effects on the position of the spectra and the associated vibronic structure.[33−36] However, these quantum methods essentially deliver stick bands (even if they are usually phenomenologically broadened), while experimental spectra are continuous and, usually, broad bands in which the vibronic progressions are partially resolved or completely hidden under a structureless line shape. In polar solvents, in particular, a major contribution to the spectral signal, i.e., the so-called inhomogeneous broadening, is due to the strong solute−solvent interactions and the consequent effect that solvent fluctuations have on transition energies.

According to Marcus's theory,[37] such broadening can be represented as a Gaussian line width whose standard deviation depends on solvent reorganization energy. We recently showed that, in polar aprotic solvents, implicit models like PCM, in combination with TD-DFT or CASSCF/CASPT2, provide a cheap and effective way to estimate such a quantity, predicting spectra in nice agreement with experiment.[15,23,38,39] Yet, implicit solvent models cannot deal with a number of situations where the molecularity of the environment must be taken into account. This is clearly the case with heterogeneous environments, such as the inside of a protein complex, the core of a lipidic membrane, the entanglement of a polymeric matrix, or the microenvironment felt by a dye attached to a semiconductor in a dye-sensitized solar cell. Moreover, implicit models may fail even in homogeneous media, if strong specific solute−solvent interactions, as for instance hydrogen bonds, exist.

One possible solution could be found in the adoption of mixed models, namely clusters, comprising the solute and a few solvent molecules embedded in a PCM *medium*. These approaches have, however, their own limitations, essentially connected with the elusive definition of such supramolecular clusters. As a matter of fact, due to the reduced strength of the intermolecular interactions with respect to the covalent ones, several solvent spatial arrangements may coexist in standard conditions, and even the number of neighbor shells explicitly included into the cluster may have important effects on the final spectral shape.[19,23]

These considerations explain why there is a compelling need for the development of novel and robust models able to combine a QM description of the solute spectrum with a molecular (explicit) description of solute−solvent interactions, and several groups are working in this direction.[21,23,25,27,40] The achievement of this final goal and the detailed understanding of the relative importance of the different effects require, however, a number of steps.

In such a framework, in this contribution we explore the performance of a computational protocol that parallels our previous work on implicit models,[15,38] with the difference that the broadening is computed with explicit models. Therefore, also in the present scheme, the final spectrum of the solvated dye will be obtained from a convolution of solute and solvent contributions.

For a more in-depth comparison of implicit and explicit approaches, we start our analysis showing, in section 2, that both protocols can be cast in the common framework of classical approximations of the solvent spectrum. In this way we also highlight that the possibility to express the final spectrum as a convolution of two separate contributions is grounded on the hypothesis that solute and solvent motions are decoupled, even though they both rearrange as a consequence of the electronic transition. While this separation is automatically fulfilled in implicit models where solvent nuclear degrees of freedom are not explicitly included, it must be enforced with explicit models. In our protocol this is done simply by running a MD simulation of the solvent around a solute molecule frozen in its ground-state (GS) equilibrium geometry. The solvent line shape is then derived from the distribution of the vertical transition energies, computed over a representative set of snapshots taken during such dynamics. In contrast, the solute line shape is obtained at room temperature by a TD quantum approach providing fully converged room-temperature spectra in harmonic approximation.[15]

As a case study, we have chosen the set of structurally related coumarin dyes sketched in Figure 1, relevant for dye-sensitized

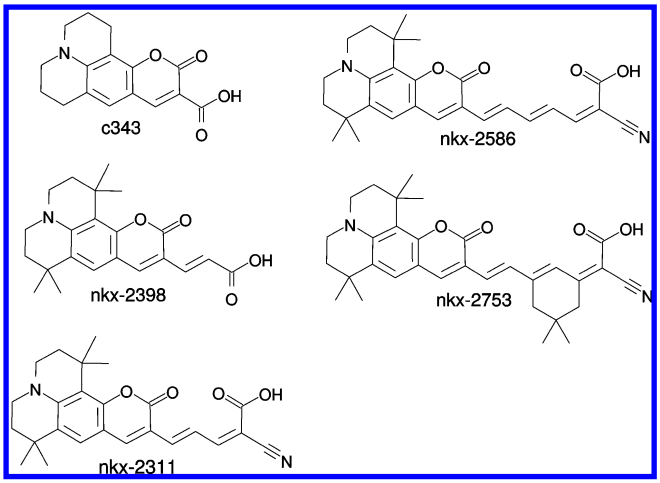

Figure 1. Structural formula of the five coumarins studied in this work.

solar cells. In ref 39 we showed that, for these molecules, the protocol based on the implicit model provides spectra in reasonable agreement with experiment, although some discrepancies remain. These systems are particularly appealing for the present study, because of the different partial charge-transfer (CT) character of their electronic transitions, which induces a strong and system-dependent broadening. Moreover, the presence, on the selected coumarins, of a number of sites (as the carboxylic and carbonyl groups or the nitrogen atom) prone to give specific interactions (H-bonds) with the solvent molecules suggests that explicit models might outperform implicit ones.

2. THEORETICAL FRAMEWORK

Let us consider an optical transition between the initial i ($|e_i\rangle$) and final f ($|e_f\rangle$) electronic adiabatic states of the solute (s),

DOI: 10.1021/acs.jctc.5b00870
J. Chem. Theory Comput. 2015, 11, 5810−5825

embedded in a medium (m). The total vibrational Hamiltonian of the solute−medium supersystem, associated with state $\kappa = i,f$, is

$$H_\kappa^{\mathrm{tot}} = H_\kappa^{(\mathrm{s})}(\mathbf{q}) + H_\kappa^{(\mathrm{m})}(\mathbf{Q}) + H_\kappa^{(\mathrm{m,s})}(\mathbf{q}, \mathbf{Q}) \tag{1}$$

$$H_\kappa^{(\mathrm{s})}(\mathbf{q}) = T^{(\mathrm{s})} + V_\kappa^{(\mathrm{s})}(\mathbf{q}) \tag{2}$$

$$H_\kappa^{(\mathrm{m})}(\mathbf{Q}) = T^{(\mathrm{m})} + V_\kappa^{(\mathrm{m})}(\mathbf{Q}) \tag{3}$$

where $\mathbf{q}$ and $\mathbf{Q}$ are convenient sets of coordinates of the solute and the medium, respectively, while $V_\kappa^{(\mathrm{s})}$ and $V_\kappa^{(\mathrm{m})}$ are their potential energy surfaces (PES) in the state κ. The line shape of the spectrum due to the transition $|e_i\rangle \rightarrow |e_f\rangle$ can be formally written in a TD framework as

$$L(\omega, T) = \frac{1}{2\pi Z_{v_i^{(\mathrm{tot})}}} \int \chi^{(\mathrm{tot})}(t, T)\, \mathrm{e}^{i\omega t}\, \mathrm{d}t \tag{4}$$

where t is the time, T the temperature, and $Z_{v_i^{(\mathrm{tot})}}$ is the vibrational partition function. The latter is obtained over the vibrational states ($|\mathbf{v}_i^{(\mathrm{tot})}\rangle$) of the solute−medium system, when the former is in its $|e_i\rangle$ electronic state.

The correlation function $\chi^{(\mathrm{tot})}(t,T)$ is

$$\chi^{(\mathrm{tot})}(t, T) = \mathrm{Tr}[\mu_{i,f}\, \mathrm{e}^{-itH_f^{(\mathrm{tot})}/\hbar} \mu_{f,i}\, \mathrm{e}^{-(\beta - it/\hbar)H_i^{(\mathrm{tot})}}] \tag{5}$$

where Tr refers to the trace over the initial states $|\mathbf{v}_i^{(\mathrm{tot})}\rangle$, $\beta = (k_\mathrm{B}T)^{-1}$, with k_B being the Boltzmann constant and $\mu_{i,f}$ and $\mu_{f,i}$ representing the matrix elements of the electric dipole between the two states $|e_i\rangle$ and $|e_f\rangle$.

To work out a practical computational protocol to estimate the solvent contribution to the spectral shape, we neglect the coupling between the solute and medium nuclear coordinates in eq 1, thus $H^{(\mathrm{s,m})} = 0$. Notice that, according to this approximation, the medium is still coupled to the optical transition, since the PESs $V_i^{(\mathrm{m})}(Q)$ and $V_f^{(\mathrm{m})}(Q)$ are in general different. However, the reaction of the solvent nuclear coordinates to the change of the solute charge density is independent of the instantaneous nuclear structure of the solute. In this approximation $\chi^{(\mathrm{tot})}(t,T)$ is simply the product of the solute ($\chi^{(\mathrm{s})}(t,T)$) and medium ($\chi^{(\mathrm{m})}(t,T)$) correlation functions:

$$\chi^{(\mathrm{tot})}(t, T) = \chi^{(\mathrm{s})}(t, T)\chi^{(\mathrm{m})}(t, T) \tag{6}$$

with

$$\chi^{(\mathrm{s})}(t, T) = \mathrm{Tr}_\mathrm{s}[\mu_{i,f}\, \mathrm{e}^{-itH_f^{(\mathrm{s})}/\hbar} \mu_{f,i}\, \mathrm{e}^{-(\beta - it/\hbar)H_i^{(\mathrm{s})}}] \tag{7}$$

$$\chi^{(\mathrm{m})}(t, T) = \mathrm{Tr}_\mathrm{m}[\mathrm{e}^{-itH_f^{(\mathrm{m})}/\hbar}\, \mathrm{e}^{-(\beta - it/\hbar)H_i^{(\mathrm{m})}}] \tag{8}$$

where the subscripts "s" and "m" indicate that the trace is taken over the solute ($|\mathbf{v}_i^{(\mathrm{s})}\rangle$) or over the medium ($|\mathbf{v}_i^{(\mathrm{m})}\rangle$) vibrational states, with $|\mathbf{v}_i^{(\mathrm{tot})}\rangle = |\mathbf{v}_i^{(\mathrm{s})}\rangle|\mathbf{v}_i^{(\mathrm{m})}\rangle$. Additionally, we made the assumption that $\mu_{i,f}$ (and therefore $\mu_{f,i}$) does not depend on the medium coordinates.

A direct consequence of eq 6 is that the total line shape can be written as a convolution of the line shapes of the solute and the medium (see, for example, ref 3),

$$L^{(\mathrm{s})}(\omega, T) = \frac{1}{2\pi Z_{v_i^{(\mathrm{s})}}} \int \chi^{(\mathrm{s})}(t, T)\, \mathrm{e}^{+i\omega t}\, \mathrm{d}t \tag{9}$$

$$L^{(\mathrm{m})}(\omega, T) = \frac{1}{2\pi Z_{v_i^{(\mathrm{m})}}} \int \chi^{(\mathrm{m})}(t, T)\, \mathrm{e}^{+i\omega t}\, \mathrm{d}t \tag{10}$$

$$L(\omega, T) = \int L^{(\mathrm{s})}(\omega - \omega') L^{(\mathrm{m})}(\omega')\, \mathrm{d}\omega' \tag{11}$$

The Hamiltonian partition in eq 1 has also implications on the moments of the spectra defined as $M_n = \int \omega^n L(\omega)\, \mathrm{d}\omega$. In particular, the average energies (i.e., the first moments $\mathcal{M}_1$) and the variances ($\sigma^2 = \mathcal{M}_2 - \mathcal{M}_1^2$) of the two line shapes $L^{(\mathrm{s})}(\omega,T)$ and $L^{(\mathrm{m})}(\omega,T)$ simply add each other in the total line shape.

As far as semi-rigid solutes are considered, a quantum calculation of the vibronic line shape is now rather standard, invoking harmonic approximation for the PESs $V_i^{(\mathrm{s})}$ and $V_f^{(\mathrm{s})}$. In fact in this approximation, analytical expressions for the finite-temperature correlation function $\chi^{(\mathrm{s})}(t,T)$ have been derived for both FC and HT approximations of the electronic transition moment $\mu_{i,f}$ (see, for example, refs 8−16, 41).

Turning to the medium, different approaches can be adopted to obtain expressions for $\chi^{(\mathrm{m})}(t,T)$ or, directly, for the line shape $L^{(\mathrm{m})}(\omega,T)$, as detailed in the following.

2.1. Classical Approximation of the Solvent Line Shape: Inhomogeneous Broadening. Due to the many possible minima and its anharmonic modes, the description of the solvent vibronic quantum states is out of reach. On the other hand, the solvent is not expected to introduce additional vibronic structures (except for the case of solute−solvent specific intermolecular vibrations, which should be included in a "clustered solute" model),[23] but mostly to shift and broaden the solute spectrum. With this picture in mind, it is convenient to derive a classical expression for the solvent line shape. To this end we start from the TD quantum expression of the line shape $L^{(\mathrm{m})}(\omega)$ in eq 10 and rewrite the correlation function in eq 8 as

$$\frac{\chi^{(\mathrm{m})}}{Z^{(\mathrm{m})}} = \mathrm{Tr}[\mathrm{e}^{-iH_f^{(\mathrm{m})}t/\hbar}\, \mathrm{e}^{iH_i^{(\mathrm{m})}t/\hbar} \hat{\rho}^{(\mathrm{m})}] \tag{12}$$

i.e., the trace over the propagators in the initial and final states multiplied by the density operator defined as $\hat{\rho}^{(\mathrm{m})} = \mathrm{e}^{-\beta \hat{H}_i^{(\mathrm{m})}}/Z^{(\mathrm{m})}$. By expanding the exponentials in eq 12 in Taylor series as a function of t, we get the following relation,

$$\begin{aligned}&\mathrm{Tr}[\mathrm{e}^{-iH_f^{(\mathrm{m})}t/\hbar}\, \mathrm{e}^{iH_i^{(\mathrm{m})}t/\hbar} \hat{\rho}^{(\mathrm{m})}] \\ &\quad \simeq \mathrm{Tr}[\mathrm{e}^{-i(H_f^{(\mathrm{m})} - H_i^{(\mathrm{m})})t/\hbar} \hat{\rho}^{(\mathrm{m})}] + O(t^3)\end{aligned} \tag{13}$$

Hereafter we make use of the approximate equivalence in eq 13, neglecting the cubic and higher terms in t, and we move to a coordinate representation, obtaining

$$\begin{aligned}L^{(\mathrm{m})}(\omega, T) = \frac{1}{2\pi} &\int \rho^{(\mathrm{m})}(\mathbf{Q}, T)\, \mathrm{d}\mathbf{Q} \\ &\int \mathrm{e}^{-i[\Delta V^{(\mathrm{m})}(\mathbf{Q}) - \hbar\omega]t/\hbar}\, \mathrm{d}t\end{aligned} \tag{14}$$

where $\rho^{(\mathrm{m})}(\mathbf{Q},T) = \langle \mathbf{Q}|\, \hat{\rho}^{(\mathrm{m})} |\, \mathbf{Q}\rangle$ is the expectation value of the density operator in the coordinate representation and we exploited the fact that $H_f^{(\mathrm{m})} - H_i^{(\mathrm{m})} = V_f^{(\mathrm{m})} - V_i^{(\mathrm{m})} = \Delta V^{(\mathrm{m})}$. Recognizing that the right-most integral in the previous equation represents a Dirac delta function, one gets

$$L^{(\mathrm{m})}(\omega, T) = \hbar \int \rho^{(\mathrm{m})}(\mathbf{Q}, T) \delta[\Delta V^{(\mathrm{m})}(\mathbf{Q}) - \hbar\omega]\, \mathrm{d}\mathbf{Q} \tag{15}$$

DOI: 10.1021/acs.jctc.5b00870
J. Chem. Theory Comput. 2015, 11, 5810−5825

where we have explicitly indicated which variables depend on the solvent coordinates, $\mathbf{Q}$, and the temperature, T.

Equation 15 has been already derived in refs 28 and 42 and represents a semi-classical approximation of the spectrum inasmuch as it is not able anymore to describe vibronic structures, but it still depends on the quantum density operator. An equivalent expression was derived by Bergsma et al.[43]

To turn eq 15 into a working expression, the Dirac delta function shall be defined in terms of the integral variables $\mathbf{Q}$. This can be achieved by exploiting the composition rule of the Dirac delta,[44]

$$\delta[f(x)] = \sum_i \frac{\delta(x - x_i)}{|f'(x_i)|} \tag{16}$$

where $f'(x)$ is the derivative of $f(x)$, and the sum runs over its roots denoted as x_i. Note that the above expression is only valid when the derivative is not zero. For a N-dimensional PES, the derivative becomes the gradient $\nabla f(\mathbf{Q})$, the roots describe an $(N - 1)$-dimensional surface so that the above sum is transformed into an integral over such surface (S). In our case $f(\mathbf{Q},\omega) = \Delta V^{(m)}(\mathbf{Q}) - \hbar\omega$, and for each ω the surface $S(\omega)$ is defined by the degeneracy condition $\Delta V^{(m)}(\mathbf{Q}) = \hbar\omega$. At each point on S, the coordinate that removes the degeneracy is parallel to the gradient $R(\mathbf{Q}) = \nabla(\Delta V^{(m)}(\mathbf{Q}))$. Finally, eq 15 can be rewritten as

$$L^{(m)}(\omega, T) = \hbar \int_{S(\omega)} \rho^{(m)}(\mathbf{Q}, T) R^{-1}(\mathbf{Q})\, d\mathbf{Q} \tag{17}$$

2.2. Practical Protocols To Compute the Solvent Broadening. *2.2.1. A Simplified Model: The Solvent as a Bath of Harmonic Modes.* In many contexts, such as electron transfer theory,[45] quantum dissipative systems,[46] and optical spectroscopy,[42] the solvent is described as an ensemble of harmonic modes reacting to the change of state of the solute. In the field of electronic spectroscopy, the simplest model assumes that the equilibrium position of the solvent mode (i) is displaced during the electronic transition, while its frequencies Ω_i remain the same. In formulas this means that $\Delta V^{(m)}(\mathbf{Q})$ is a simple linear function of the solvent coordinates. As detailed in the Supporting Information (SI), for this model, one easily gets that the solvent contribution to the spectrum is a Gaussian centered at E_V,

$$L^{(m)}(\omega, T) \propto \exp\left[-\frac{(\hbar\omega - E_V)^2}{2(\sigma^{(m)})^2}\right] \tag{18}$$

Moreover, in the high-temperature classical limit ($\hbar\Omega_i \ll K_B T$, for each mode i), the variance of the Gaussian is

$$(\sigma^{(m)})^2 = 2k_b T E^r \tag{19}$$

where E^r is the solvent reorganization energy, i.e., the difference of the solvent energy before and after equilibration with the solute density on the final electronic state.

It is noteworthy that eq 19 coincides with the classical ($\hbar\Omega_i \ll k_b T$, for each mode i) limit of the quantum variance obtained by analytical derivation of the spectral moments.[11,28,47] Moreover, this expression is identical to what obtained by Marcus theory on the grounds of a particle description of polar media,[48−50] assuming that the solute and solvent nuclear degrees of freedom are not coupled and treating the latter according to classical statistics.

2.2.2. Implicit Solvent Models. Equation 19 has the interesting property to connect the broadening induced by the solvent to a single collective quantity, i.e., the solvent reorganization energy induced by the optical transition of the solute. Implicit solvent models like PCM[32] provide a straightforward route to compute E^r as the difference of the "neq" (non-equilibrium) and "eq" (equilibrium) transition energies (E_V) of the final electronic state,

$$(\sigma_{im}^{(m)})^2 = 2k_b T(E_V^{neq} - E_V^{eq}) \tag{20}$$

In the framework of PCM and of other continuum solvation models, "neq" and "eq" time regimes are simply ruled by two different dielectric constants. In the "neq" case, the reaction field due to the fast solvent degrees of freedom depends on the dielectric constant at optical frequency (ε_{opt}, usually related to the square of the solvent refractive index, $\varepsilon_{opt} = n^2$). Equilibrium solvation is instead ruled by the static dielectric constant.

Within the validity of the initial hypothesis, i.e., that solvent and solute movements are separated, the estimate of $\sigma_{im}^{(m)}$ should not drastically depend on the solute geometry, and, in line with the procedure outlined for explicit solvent models, these data are computed at the equilibrium geometry of the solute in the initial state.

The expression in eq 20 has been already adopted in few cases, computing E_V^{neq} and E_V^{eq} with the state-specific implementation of PCM within TD-DFT (SS-PCM/TD-DFT)[51−53] or with CASSCF/CASPT2.[15] In combination with vibronic line shapes simulated from TD-DFT PES, SS-PCM/TD-DFT broadenings provided absorption spectra in nice agreement with experiment for several systems, either in aprotic solvents[15,27,38,54] or in water.[23,27] In this latter case, a cluster model was adopted. Very recently this protocol provided spectra in reasonable agreement with experiment also for the series of coumarin dyes investigated here.[39]

2.2.3. Explicit Solvent Models. In order to obtain a working protocol to estimate the solvent broadening from explicit solvent models, we consider again eq 17. It should be noticed that in the classical limit (high temperature), the density becomes the Boltzmann distribution, ρ_B, which can be sampled by classical methods, as MD or Monte Carlo. Moreover, for computational convenience, we assume that the factor R is a constant. This is strictly true for the simplified model discussed in section 2.2.1. With these approximations, the final form for the classical expression for $L^{(m)}(\omega,T)$ is

$$L^{(m)}(\omega, T) \propto \int_{S(\omega)} \rho_B^{(m)}(\mathbf{Q}, T)\, d\mathbf{Q} = \hbar\rho^{(m)}(\omega, T) \tag{21}$$

where $\rho^{(m)}(\omega,T)$ is the density of vertical transition energies, $\hbar\omega$, regardless the conformation. Therefore, a practical way to simulate $L^{(m)}(\omega)$ is to perform a conformational sampling of the solvent according to $\rho_B(Q,T)$, compute the vertical energy at each point, and then build a histogram to get an approximation to $\rho^{(m)}(\omega,T)$.

A direct application of eq 21 could allow us to obtain a full line shape for $L^{(m)}(\omega)$ directly from the aforementioned histogram. However, starting from eq 13, it is possible to show that even when $\rho^{(m)}(Q,T)$ is the exact quantum distribution, a classical approximation of the spectrum reproduces only the average frequency and variance of the quantum spectrum, but not its asymmetry.[28] Therefore, for the convolution with the solute spectrum we adopted a more conservative procedure, neglecting the fine details of the sampled distributions

DOI: 10.1021/acs.jctc.5b00870
J. Chem. Theory Comput. 2015, 11, 5810−5825

$\rho^{(m)}(\omega,T)$ and simulating $L^{(m)}(\omega,T)$ with a Gaussian function with the same standard deviation ($\sigma_{ex}^{(m)}$) as $\rho^{(m)}(\omega,T)$.

3. COMPUTATIONAL DETAILS

3.1. MD Simulations. MD simulations were performed for each of the dyes considered in the present work (see Figure 1) on systems composed of one solute and about 8000 ethanol (EtOH) molecules. For the smaller c343 dye, additional simulations were carried out in acetonitrile (ACN) and dichloroethane (DCE) solvents. To enforce the separation of solute and solvent motions (i.e., $H^{(s,m)} = 0$), necessary to apply eq 11, during the MD simulation the solute is kept frozen at GS equilibrium geometry, thus only $\rho_B^{(m)}(\omega,T)$ is sampled.

All MD runs were performed using the GROMACS-4.5 software.[55] To unravel the effect of different descriptions of the solute−solvent interactions on the adopted explicit models, several sets of force field (FF) parameters were assembled. As far as the medium is concerned, all investigated solvents were modeled through either the Generalized AMBER Force Field (GAFF)[56] or the All-Atom Optimized Potentials for Liquid Simulations (OPLS-AA),[57] taking the parameters from the Virtual Chemistry database.[58]

Turning to the solute, three sets of parameters were tested. First, GAFF Lennard-Jones (LJ) parameters, obtained for each coumarin with the ANTECHAMBER program[56] were coupled with RESP point charges[59] obtained at two different levels of theory, either from the HF/6-31G(d) density in vacuo (set I) or with CAM-B3LYP/6-31G(d) along with PCM (set II). While the former strategy closely follows the original RESP recipe, the latter appears more coherent with the level of calculation used in the subsequent TD-DFT calculations. Next, OPLS/AA LJ parameters were selected, and employed in simulations jointly with CM5 charges, obtained from the CAM-B3LYP/6-31G(d) density in PCM (set III).[60] A summary of the different parametrization strategies is given in Table 1.

Table 1. Parameterization Strategies for the Adopted FFs

set	LJ	charges
I	GAFF	RESP/HF
II	GAFF	RESP/CAM
III	OPLS	CM5/CAM

In all MD simulations, performed in the canonical (NVT) ensemble, short-range interactions were truncated at a cutoff distance of 11 Å. Long-range electrostatics was treated with the PME algorithm.[61] Temperature (T) was kept constant through the Berendsen[62] and Nosé−Hoover[63] algorithms, for equilibration and production runs, with coupling constants τ_T of 0.1 and 1.0 ps, respectively. All runs were extended for around 6 ns with a time step of 2 fs, constraining the bonds with the LINCS algorithm.[64]

3.2. Sampling. In the SI we report in detail the preliminary tests we performed to establish the protocol to extract the set of configurations for QM/MM calculations. The tests were tailored to ensure that the number of frames, the export frequency and the size of the explicit solvent layer around solute in every extracted snapshot were adequate to obtain converged and unbiased data. We further checked that inclusion of a continuum model outside the explicit sphere does not change the results. After such preliminary studies, the final protocol can be summarized as follows.

For each system, the coordinates of selected molecules are exported every 30 ps along the 6 ns MD simulations, thus generating ensembles of 200 configurations. This export rate provides uncorrelated snapshots and the total number of them was enough to ensure the convergence of the property under consideration: the standard deviation corresponding to the distribution of E_V.

Each snapshot consists of the solute surrounded by an explicit solvent sphere, whose radius was set to 40 Å. Although we acknowledge the usefulness of using the PCM model outside such explicit solvent sphere, we decided not to use it to avoid technical problems that may arise when the PCM cavity is too large. As shown in the SI, the solvent layer of 40 Å was large enough to provide energies practically identical to those obtained with a smaller solvent layer surrounded by a PCM medium.

The system is partitioned into a QM and a MM region. The former, treated at TD-DFT level,[65] always includes the coumarin dye and, in some cases, the closer solvent molecules. The rest of the system is treated at MM level, taking each solvent atom into account as a single point charge, whose value is given by the partial charges adopted during MD simulations.

3.3. QM Calculations. Electronic structure calculations were performed with the Gaussian09 software,[66] making use of DFT and TD-DFT for the GS and ES, respectively. All calculations were carried out with the range separated hybrid functional CAM-B3LYP[65] in conjunction with the 6-31G(d) basis set. This protocol is computationally convenient since it employs a rather small basis set with a split-valence double-ζ quality which does not include diffuse functions. The adoption of such basis set has been shown to provide spectral line shapes in nice agreement with the experiment for few coumarin dyes,[36,39] and it has been extensively tested with success on the vibronic spectra of a benchmark set of 20 π-conjugated systems in combination with the same functional CAM-B3LYP adopted here.[67] Despite this comforting evidence, we preliminarily investigated the effect of the extension of the basis set on the chosen molecules. In the SI we show that for c343 a larger basis set, 6-311+G(d,p), predicts a red shift of the vertical energies by ca. 0.12 eV, keeping however practically unaltered the width and shape of the distribution. Therefore, in consideration of the large amount of QM/MM calculations required to compute the necessary σ for all investigated systems, for the QM layer the smaller 6-31G(d) basis set was used.

3.4. Spectral Line Shapes. Vibrationally resolved spectra have been computed in FC approximation, according to the same recipe followed in ref 39. The harmonic PESs have been modeled by using Adiabatic Hessian (AH) approach,[68] that expands each PES around its own equilibrium position and accounts for Duschinsky effect.[69] We used internal coordinates (bonds, angles and dihedrals obtained from the Z-matrix) to describe the normal modes, which is advantageous when facing large displacements between the initial and final state geometries.[70,71] Solvent effects on equilibrium geometries and Hessians have been included by the PCM model, using for the excited states (ESs) the standard implementation of PCM/TD-DFT, based on the Linear Response theory (LR-PCM/TD-DFT)[51,72] in "neq" regime. Notice that adoption of PCM allows to introduce mean-field (not broadening) solvent effects on the solute vibronic shape.

ES PESs utilized for spectra calculation were vertically translated in order to match the adiabatic energy difference predicted by SS-PCM calculations, i.e., the difference between

DOI: 10.1021/acs.jctc.5b00870
J. Chem. Theory Comput. 2015, 11, 5810−5825

the "neq" ES energy and the "eq" GS energy in their respective minima. Full-convergence spectra at room temperature were obtained exploiting analytical expressions of the finite-temperature time-correlation function, χ (eq 5), for harmonic PESs;[8−16,41] see ref 15 for implementation details. All the spectra calculations were performed by a development version of our code FCclasses.[73,74]

Within the explicit solvent models, the solvent line shape, $L^{(m)}(\omega,T)$, is evaluated, as detailed in section 2.2.3, from the distribution of the vertical transition energies, computed over the snapshots extracted according to the afore-described QM/MM strategy. More specifically, CAM-B3LYP/6-31G(d) was employed for the QM region and the same point charges adopted in simulations were used for the MM part. The histograms for the vertical energy distribution were obtained for each set of FFs using a bin width of 0.025 eV. While the histograms give an idea about how well the data follow a normal distribution, the spectral line shape of the medium, $L^{(m)}(\omega)$, is simulated as a Gaussian function having the same standard deviation, as discussed in section 2.2.3.

The total spectrum, $L^{(tot)}(\omega,T)$, is obtained convoluting the quantum spectrum of the solute, with the solvent classical broadening. Both PCM and QM/MM calculations provide transition energies that already consider the solvent effect, and they are in general different. In order to avoid double counting of the solvent effect, and since in this contribution we focus on the comparison of spectral shapes arising from broadenings obtained with either PCM or explicit models, in the following, for internal coherence, we fix the moment of the total spectrum at the value of the $L^{(s)}$ first-moment computed on the grounds of SS-PCM/TD-DFT data (i.e., we set to zero the first moment of the convoluting Gaussian $L^{(m)}(\omega)$). As shown in the following, SS-PCM/TD-DFT and QM/MM average frequencies become very similar increasing the number of solvent molecules included in the QM layer.

We already preliminary tested an approach similar to those described above in ref 40. Herein, after presenting these approaches in detail, we explore their performance for coumarin dyes in EtOH, adopting different FFs and comparing their predictions with those of implicit models. Very recently, similar strategies were elaborated by Zalesny et al.[21] and used to investigate heterocyclic ketoimine difluoroborates in chloroform and dimethylformamide.

4. RESULTS

We start presenting a detailed analysis of the role played by different factors in determining the estimation of the inhomogeneous broadening. For these extensive tests we focused on the small c343 dye.

4.1. Analysis of Different Contributions to the Calculation of the Broadening. *4.1.1. Effect of the Force Field on the Sampling.* In Table S1, the three sets of FF parameters are reported. From the MD simulations in EtOH at 300 K, performed using the three sets, differences arise in the hydrogen bond (HB) network resulting from the simulation with set I and II with respect to set III parameters. This is revealed by the radial distribution function (RDF) of solvent molecules around the oxygen atoms of the dye in Figure 2; a more complete description of the distribution of the solvent around the solute is given by the spatial distribution functions in Figure S3. Indeed, the simulations with RESP charges, either obtained using HF (set I) or CAM-B3LYP (set II), result in stronger hydrogen bonds as compared with those obtained with

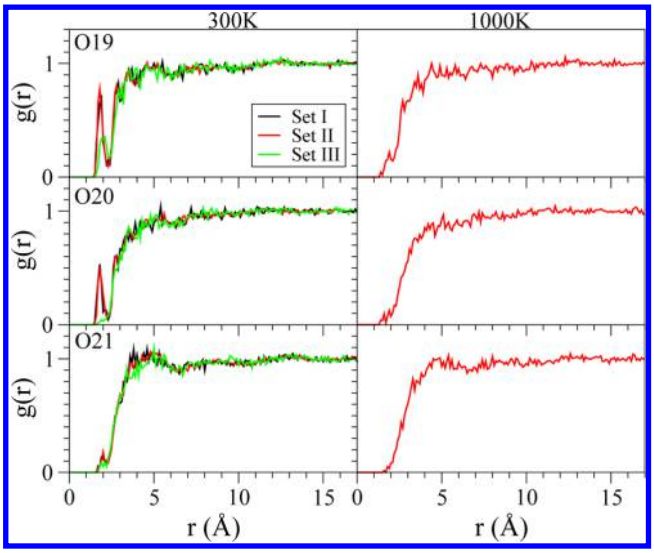

Figure 2. Radial distribution functions, $g(r)$, corresponding to coumarin oxygen-EtOH pairs, analyzing each oxygen in the coumarin c343 separately. All distributions were computed along the MD simulations, performed either at 300 K (left) or 1000 K (right) using the three sets of FF parameters adopted in this work. Snapshots are taken every 30 ps.

set III. This different behavior can be traced back to both the set of charges for the coumarin dye, which is generally larger, in absolute value, for the RESP scheme and the more attractive LJ potential yielded by EtOH GAFF parameters.

A deeper insight on the interaction between the coumarin and the solvent can be gained by inspecting the evolution of the Coulomb and LJ intermolecular potential along the simulation. In Figure 3 we show, for MD runs carried out with FF sets II

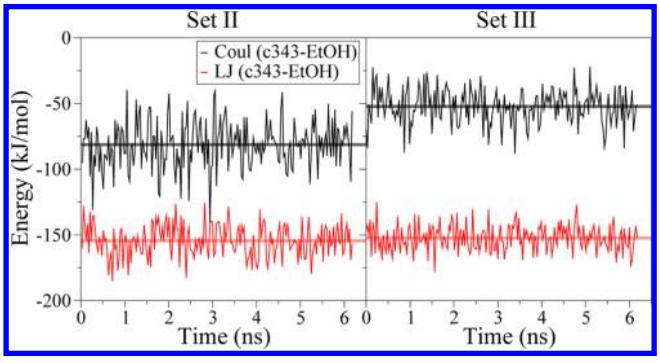

Figure 3. Coulomb (Coul) and Lennard-Jones (LJ) interactions between the coumarin c343 and the solvent molecules (EtOH) along the MD simulations carried out with FF sets II and III.

and III, the interactions between the dye and all the surrounding solvent molecules. We do not consider set I since it provided a very similar sampling to set II, as indicated by the RDF. It can be observed that, for each FF set, both Coulomb and LJ terms lead to an overall attractive interaction, the latter being two to three times more intense than the former. More precisely, the LJ contributions are very similar for the two sets (~150 kJ/mol), whereas, as could be expected from the simple analysis of the point charges discussed above, Coulomb interactions are stronger for set II (~75 kJ/mol) with respect to set III (~50 kJ/mol).

DOI: 10.1021/acs.jctc.5b00870
J. Chem. Theory Comput. 2015, 11, 5810−5825

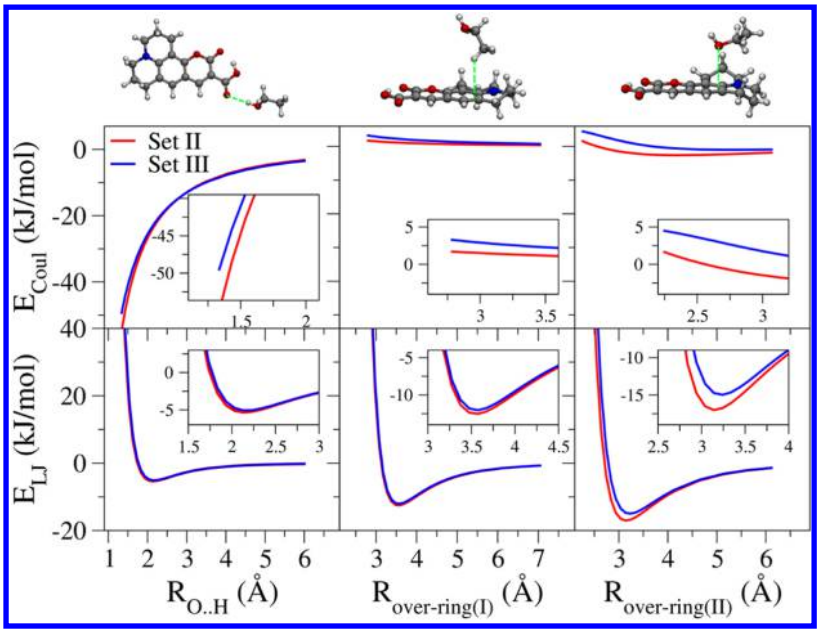

Figure 4. Coulomb (Coul) and Lennard-Jones (LJ) interactions, computed with FF sets II and III, at different distances along three paths connecting the dye and one solvent molecule (schematic description above the graph). Insets: zoom around the well of the LJ potential.

Such analyses provide a global picture of the solute−solvent interaction and, although useful to pick up differences between the sampling arising from the use of different FFs, they do not provide any information about the specific interaction sites between the solute and the solvent.

In order to inquire the intermolecular interactions at specific locations relevant for the transition energy (see the Discussion section), in Figure 4 we report the Coulomb and LJ terms computed with sets II and III, considering three different paths in which an EtOH molecule approaches the c343 dye. The three paths describe either a hydrogen bond formed between the lactone carbonyl oxygen and the hydroxyl hydrogen in EtOH (left panel) or the interaction between the aliphatic rings of the coumarin and either the methyl (central panel) or the hydroxyl (right panel) moiety of the EtOH molecule.

By comparing the role of the two contributions in the considered paths, it appears that, for both FF sets, the Coulomb term is drastically reduced when the EtOH molecule approaches the dye toward the aliphatic rings (second and third paths), whereas a significant charge−charge contribution characterizes the interaction between the OH group of the solvent and the coumarin's oxygen (first path). Turning to the comparison between the two FF sets, the LJ contributions are very similar for all sets at all positions, while larger differences arise in the Coulomb term, as the solvent and solute come closer. More specifically, in agreement with the stronger hydrogen bonds observed for set II, the Coulomb attraction is larger using the parameters of this set. This latter observation still holds for the last of the paths considered, when the hydroxyl group of the EtOH molecule approaches the aliphatic part of the dye, although in this case not negligible differences between the two sets appear also in the LJ contributions. Considering the similarity of the dye LJ parameters in sets II and III, this last feature can be traced back to the different description, in terms of LJ parameters, of the OH group, whose oxygen atom has a smaller σ and a larger ε in set II (see Table S2).

4.1.2. Effect of the Force Field on the Prediction of the Inhomogeneous Broadening. Figure 5 compares the vertical energy distributions obtained with the three FF sets (see Table 1), when all solvent molecules were included in the MM region of QM/MM calculations.

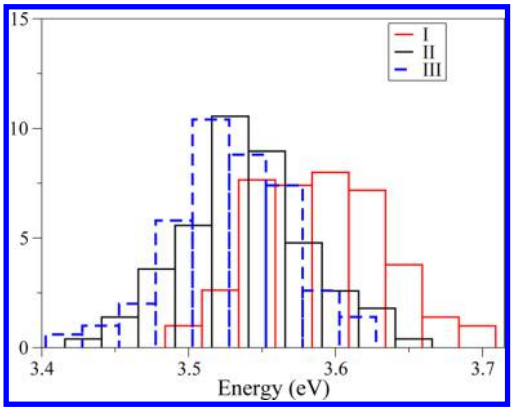

Figure 5. Ev histograms obtained by computing the transitions along the MD simulations with the three FF settings for c343. Solute treated at TD-DFT level with CAM-B3LYP/6-31G(d) and all solvent atoms as point charges according to each scheme.

The three distributions appear rather symmetric and bell-shaped; therefore they do not deviate remarkably from the Gaussian function chosen to represent the spectral line width. Table 2 collects, for each distribution, the first moment (i.e., the distribution average energy, μ) and the standard deviation $\sigma_{ex}^{(m)}$ (connected to the second moment). The latter is 0.044 eV for set I and II and 0.040 eV for set III, indicating that the three approaches lead to similar solvent-induced broadenings. In the SI we evaluate the error on $\sigma_{ex}^{(m)}$, showing that it is always on the order of 10^{-3} eV.

This notwithstanding, the first moments obtained with sets I−III do show appreciable differences. In particular it is noteworthy that μ = 3.54 eV with set II and 3.59 eV with set I.

DOI: 10.1021/acs.jctc.5b00870
J. Chem. Theory Comput. 2015, 11, 5810−5825

Table 2. First and Second Moments of the Distribution of Vertical Energies Computed on the Snapshots Extracted from MD Trajectories Using the Different Sets of FF Parameters Reported in Table 1, QM/MM Partitions, and Temperatures

FF set	partition[a]	T (K)	μ (eV)	$\sigma_{ex}^{(m)}$ (eV)
I	noQMsol	300	3.59	0.044
II	noQMsol	300	3.54	0.044
III	noQMsol	300	3.53	0.040
II	QMsol_polar	300	3.51	0.045
II	QMsol_r3A	300	3.40	0.045
II	QMsol_r6A	300	3.36	0.044
II	noQMsol	1000	3.59	0.060

[a]Solute at QM level and different partitions for the solvent: all as point charges (noQMsol), including the QM region solvent molecules within 3.5 Å from polar atoms of the solute (QMsol_polar), and within either 3 Å (QMsol_r3A) or 6 Å (QMsol_r6A) from any atom of the solute.

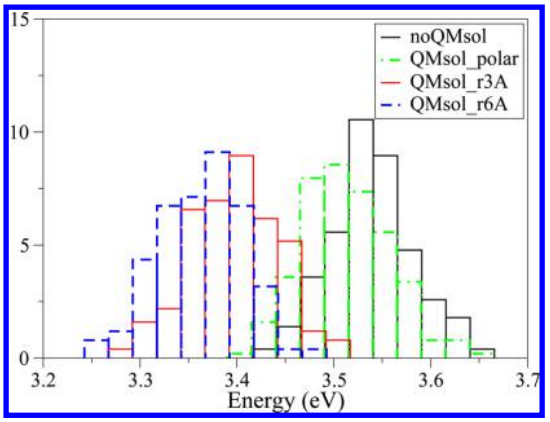

Figure 6. E_V histograms obtained by computing the transitions along the MD simulations carried out with set II of FF parameters. The solute is treated at TD-DFT level with CAM-B3LYP/6-31G(d), but with different partitions for the solvent (see footnote on Table 2).

In fact the same solvent point charges (GAFF) are used in the MM partition of the QM/MM calculations, and the only difference resides in the spatial distribution, extracted from the MD trajectories. This indicates that although the parameters of set I and II provide samplings which seem very similar from inspection of the RDF (Figure 2) and spatial distribution functions of the polar atoms (SI), their differences are large enough to produce a systematic shift of the distribution of vertical energies. This fact highlights the sensibility of the spectroscopic properties to the conformational details.

Regarding the distribution obtained with set III, its first moment (μ = 3.53 eV) lies close to that obtained with set II although, in this case, the RDF documents a remarkably different hydrogen-bonding pattern. These results suggest that the impact of the hydrogen bonds on the sampling does not play a distinguishing role on the solvent broadening.

4.1.3. Effect of the QM/MM Partition. In this section we evaluate the effect of QM/MM partition on the estimate of the solvent broadening, adopting three possible definitions of the QM layer. To reduce the computational burden, these tests were only performed on snapshots taken from the simulation with the set II of parameters. This set was selected since it predicts stronger hydrogen bonds and is therefore well suited to check whether the effect of H-bonds on the sampling has an impact on solvent broadening. Concretely, the solvent molecules included in the QM layer are those within 3.5 Å from the polar groups of the coumarin (QMsol_polar) and those within 3 Å (QMsol_r3A) or 6 Å (QMsol_r6A) from any atom of the solute.

In Figure 6, the distributions of the vertical energies computed with these three schemes are shown and compared with the results obtained accounting for all solvent molecules at MM level. As the number of solvent molecules in the QM region increases, the distribution is red-shifted while its standard deviation is almost unaltered. Interestingly, the inclusion of the solvent molecules close to the polar groups (QMsol_polar) induces only a slight red-shift of 0.03 eV with respect to the full-MM solvent, while a larger shift is observed when a whole layer of solvent molecules is treated at QM level. Indeed, a QM layer of 3 Å leads to an additional red-shift of ~0.11 eV respect to the QMsol_polar values. Enlarging the solvent layer treated at QM level to 6 Å further red-shifts the distribution by 0.04 eV, leading to a final μ = 3.36 eV. It is noteworthy that the latter value is very close to the vertical energy computed with the SS-PCM/CAM-B3LYP/6-31G(d) protocol in the "neq" regime, 3.35 eV, providing a support to the reliability of SS-PCM/TD-DFT calculations. A rationale for this trend can be found noticing that PCM involves the polarization of the solvent charges, therefore the predictions of implicit and explicit models become similar only when an increasing number of explicit solvent molecules can be polarized, as it happens when they are included in the QM layer.

To conclude the discussion of the different QM/MM partition, we highlight a possible issue arising when solvent molecules are included in the QM layer in a TD-DFT calculation. In fact, spurious CT states between the solute and the solvent might take place.[75] This flaw is expected to be alleviated by using range corrected functionals as CAM-B3LYP adopted here. We actually checked that our results are not biased by the occurrence of solute−solvent CT states.

Summarizing the results of section 4.1, it is noteworthy that the first moment appears to be more sensitive than the standard deviation to the details of the solvent distribution due to the different FF, to the QM effects of the first solvent shell and to the basis set adopted in the electronic calculation (SI).

4.2. Comparison with Experiment: Performance of Explicit vs Implicit Models. Experimentally, the spectral broadening due to a polar solvent is usually estimated by comparing the shape of spectra in apolar and polar solvents (see, for example, refs 30 and 31). This approach, which is based on the approximation that the vibronic structure of the solute is independent of the solvent, cannot be applied for the series of coumarin dyes investigated here because in non-polar solvents they undergo aggregation.[76,77] Therefore, in the present work the comparison between experimental and computational results is limited to the global line shape of the spectra in polar solvents.

In a previous work on these dyes,[39] we showed that the convolution of the vibronic shape of the solutes with the Gaussian broadening estimated with SS-PCM provides spectral shapes in nice agreement with experiment. This is witnessed in Figure 7 where we report the simulated line shape for all dyes with both the implicit (top)[39] and explicit (bottom) models, along with the experimental line shapes taken from the experiments.[78−81]

DOI: 10.1021/acs.jctc.5b00870
J. Chem. Theory Comput. 2015, 11, 5810−5825

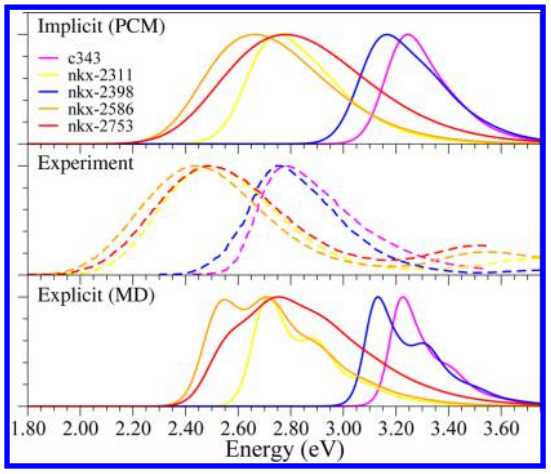

Figure 7. Vibronic spectra of all coumarins considered in this work convoluted with the solvent line shape (Gaussian) estimated with the PCM model (top panel) and with the explicit QM/MM model presented in this work (bottom panel). The experimental line shapes from refs 78−81 are included in the central panel.

Here, we consider the same vibronic spectra reported in ref 39 (and for convenience in the SI) for the investigated dyes and we estimate the solvent broadening with explicit models by applying the protocol described above with parameter set II, which predicts similar broadenings as the other two sets.

Inspection of Figure 7 indicates that implicit and explicit models provide a similar qualitative trend, both predicting that the spectral width increases with the size of the dye, which is also associated with a larger polarity change during the transition (electric dipole differences are given in Table 3).

Table 3. Standard Deviation of the Gaussian Function Representing the Solvent Line Shape Estimated with Both Implicit ($\sigma_{im}^{(m)}$, Ref 39) and Explicit ($\sigma_{ex}^{(m)}$) Models; Change in Dipole Moment between Initial and Final States Is Also Reported

dye	$\sigma_{im}^{(m)}$ (eV)	$\sigma_{ex}^{(m)}$ (eV)	$\mu^{ES} - \mu^{GS}$ (D)
c343	0.068	0.043	4.2
nkx-2398	0.075	0.039	5.4
nkx-2311	0.087	0.050	7.8
nkx-2586	0.114	0.060	11.5
nkx-2753	0.129	0.064	12.2

On a more quantitative ground, some clear differences emerge. On the one hand, data in Table 3 indicate that the solvent σ predicted by the explicit model are systematically and remarkably smaller that those computed with the implicit one. As a consequence while SS-PCM broadenings lead to the structureless bands very similar to those observed in experiment, the smaller solvent broadenings computed with the explicit model give rise to final spectra that still show a vibrational structure, in contrast with the experimental observations (Figure 7).

On the other hand, a detailed comparison with experiment suggests a more complex scenario, pointing out that the explicit model appears to better catch some relative changes. For instance, consider nkx-2398 and c343: the standard deviation of their vibronic contribution to the spectra are respectively 1256 and 1009 cm^{-1};[39] moreover, the implicit model predicts[39] that nkx-2398 exhibits a larger broadening with respect to c343, while the explicit model indicates the opposite. The analysis of the experimental line shapes given in Figure 7, reveals that the spectra of c343 is indeed broader than that of nkx-2398 (the full widths at half-maximum (fwhm) are respectively 3130 and 2960 cm^{-1}),[39] thus agreeing with the qualitative trend given by the explicit model.

C343 is probably the most studied dye in the series and data in several solvents are available in literature. This gave us the possibility to extend the investigation of the performance of the explicit model of the broadening in ACN and DCE, the two aprotic solvents already considered with the implicit model in ref 39. Table 4 reports the standard deviations corresponding to

Table 4. Spectra of c343: Standard Deviation of the Broadening Induced by Different Solvents

solvent	$\sigma_{im}^{(m)}$ (eV)[39]	$\sigma_{ex}^{(m)}$ (eV)
EtOH	0.068	0.044
ACN	0.070	0.042
DCE	0.061	0.037

the implicit and explicit models. In keeping with the results for all the coumarins in EtOH, the explicit approach provides standard deviations significantly smaller than those obtained with the implicit model. However, a further noteworthy difference between implicit and explicit approaches is observed looking at the qualitative trend: while in the implicit model the predicted broadening increases with the polarity of the solvent and is larger for ACN than for EtOH, the opposite happens within the explicit model, in line with what is observed in experiment where the fwhm is 2360 and 3130 cm^{-1} in ACN and EtOH, respectively.[39]

Together with the difference between c343 and nkx-2398 discussed above, this result suggests that, since it accounts for specific interactions between the dye and the solvent molecules, the explicit model is able to better capture the relative changes due to subtle differences between the dyes and/or the solvents.

5. DISCUSSION

A straightforward interpretation of the results reported in the previous section is that the adopted explicit model contains some source of inaccuracy, which causes the broadening underestimation. We can exploit the detailed information on the effects of the FF on the MD simulation to further test this hypothesis. To that end, let us turn back to the analysis of the FF introduced in section 4.1 for the smallest dye c343, and further exploit the potentiality of the atomistic description of the solvent, unavailable with implicit models, to achieve a detailed understanding of the solute−solvent interactions more involved in the broadening.

Within explicit solvent models, the width of the spectra might depend on both the sampling arising from the MD simulation and/or the subsequent TD-DFT calculations. The effect of the functional/basis on the spectra of this family of coumarins has already been investigated in detail in a previous work,[39] showing the need of range-separated functional, as the one adopted in this work. Regarding the QM/MM partition and MM models, our analysis in section 4.1, already reveals that these details affect the first moment but only marginally the broadening.

Regarding the effect of the MD simulation, all samplings obtained with the three FF sets led to practically the same broadening and only minor variations of the first moment, as

DOI: 10.1021/acs.jctc.5b00870
J. Chem. Theory Comput. 2015, 11, 5810−5825

shown in Figure 5 and Table 2. Therefore, in order to further explore the impact of the sampling, we set up a simulation that enforces a clearly different ensemble as compared with those shown in the previous section. Concretely, we carried out an additional simulation under artificial drastic conditions, obtained by imposing a temperature of 1000 K with the volume corresponding to that at 300 K. Such conditions have a significant effect on the sampling as already revealed by the changes observed in the corresponding RDF shown in Figure 2, where the peak related to the H-bonds practically disappears.

In Figure 8, the distribution of vertical energies resulting from this sampling is compared with that obtained at 300 K.

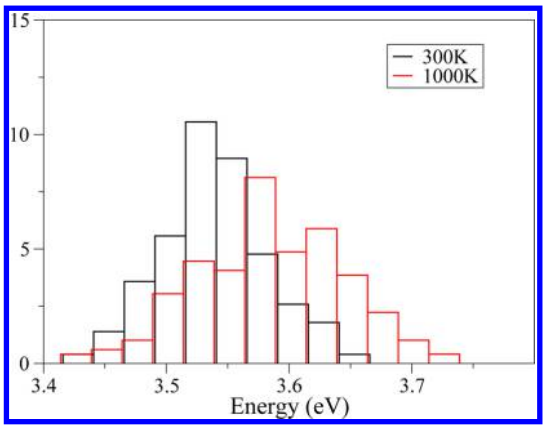

Figure 8. E_V histograms obtained for c343, with TD CAM-B3LYP/6-31G(d) and all solvent atoms treated as RESP(CAM) point charges. The sampling was generated at either 300 and 1000 K, using the same volume in both cases.

The distribution at 1000 K actually predicts a significant change of the vertical energy distribution, which has a slightly blue-shifted first moment μ and a larger standard deviation (0.06 eV). The latter confirms the significant effect of the sampled solvent configurations on the final spread of the line shape.

The fact that the solvent broadening is connected both to the density on the solute in the initial state (since it affects solvent fluctuations) and to its change upon transition (reported for c343 in EtOH in Figure S2), is indeed rather intuitive. Yet, the atomistic description of the solvent allows in principle to analyze in detail the origin of the solvent broadening and individuate the solute−solvent interactions that give the larger contribution to this phenomenon. In practice, however, given the large amount of degrees of freedom for the solvent, finding a single parameter able to make the connection between solvent conformation and the energy of the spectroscopic transition is not trivial. Here, we have resorted to the electrostatic potential generated by the solvent charges around the solute.

In the upper panel of Figure 9 the QM-computed vertical energies are reported for each of the 200 snapshots extracted from simulations performed at 300 (left) and 1000 K (right). Furthermore, in the lower panels we also display the solvent electrostatic potential over the van der Waals surface of c343 for selected snapshots, corresponding to the highest and lowest vertical energies at 300 and 1000 K (additional conformations are shown in the SI). By inspection of Figure 9, the correlation between the resulting vertical energies and the potential arising from each solvent conformation becomes rather clear and appears connected to the CT character of the spectroscopic transition (see the difference density in Figure S2). In such cases, it is well known that the presence of a polar solvent stabilizes the more polar final ES of coumarins more than their initial GS, resulting in a lower transition energy with respect to the vacuum. In fact, as far as the results at 300 K are concerned, the snapshots yielding the lowest transition energies (cases C and D) are those where the effect of the electrostatic potential due to the solvent is larger, due to the proximity of the EtOH molecules to the dye. More specifically, as evidenced by the pictorial representation of Figure 9, in both cases the solvent generates a negative potential where there is an electron depletion (aliphatic rings) and a positive one around the area where there is an electron enrichment (within the ring with the carboxylic oxygen atoms). Conversely, when the average distance of the closest solvent molecules increases, and the absolute value of the potential is consequently reduced, the energy of the transition is significantly higher (cases A and B).

Turning to the results obtained at 1000 K, from the direct comparison between the top left and right panels of Figure 9, it appears that the wider distribution achieved at the higher temperature and the slight increase of the average value, stem from the occurrence of higher vertical energy transitions (cases E and F), whereas the lower bound (cases G and H) does not differ from the one found at 300 K. This should not be surprising, since the minimum distance configurations at which solvent molecules and the dye can be found, responsible for the lowest transition energies, are defined by the repulsive branch of the solute−solvent interaction potential, which does not depend on temperature and is described by the same FF parameters in both simulations. Conversely, at 1000 K the solvent molecules describe larger fluctuations, leading to situations where the potential around the molecule is significantly lowered, resulting in the higher vertical energy limit observed at this temperature.

Although generated with intentionally anomalous conditions, the above results prove that a sampling where the solvent molecules fluctuate on a larger scale around the solute provide configurations with higher energy and, eventually, results in a wider solvent line shape. Therefore, the key question is whether samplings characterized by larger fluctuations may be predicted in standard environmental conditions by using a more refined model to describe the system. In other words: is it possible that FF inaccuracies might reflect in a not reliable sampling and, therefore, in the underestimated broadening? We focus on the ability of the FF to account for the solute−solvent interactions, by comparing the intermolecular MM potential computed (with either FF set II or III) with the curves obtained through DFT calculations performed with the Grimme's D3 dispersion corrections.[84,85] More specifically, we use CAM-B3LYP-D3/6-31G(d), and also apply the counterpoise method to correct the basis set superposition errors (BSSE). We should note that the dispersion terms provided by Grimme et al.[84] were derived by fitting the energies computed with a more extended basis set, def2-QZVP, without applying the counterpoise correction. Our tests reported in the SI (see Figure S11) show that, in almost all cases, our less demanding procedure gives values very similar to those obtained with the settings used by Grimme. The cases where the differences become relevant are those where the BSSE is quite significant even with the large def2-QZVP basis set, rising a warning on the calculation. Notably, the general discussion below is not significantly affected by these problematic points. We compute the interaction energy between the coumarin and a single molecule of EtOH placed

DOI: 10.1021/acs.jctc.5b00870
J. Chem. Theory Comput. 2015, 11, 5810−5825

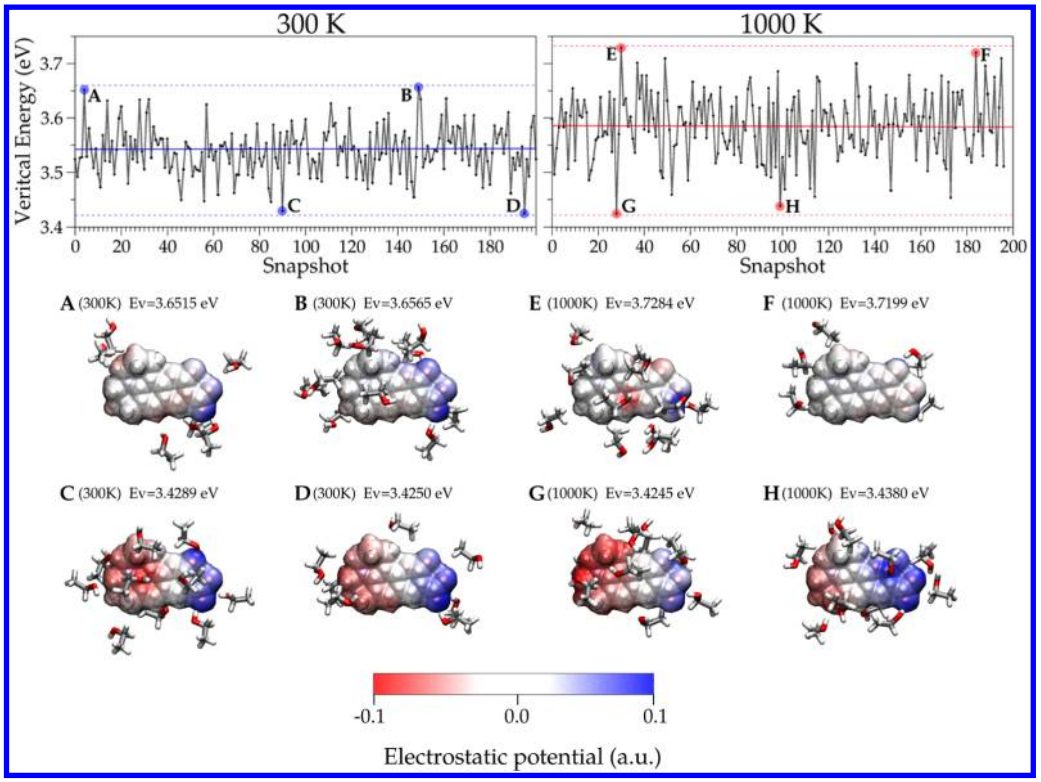

Figure 9. Variation of the vertical energy of coumarin c343 in EtOH, computed for the snapshots extracted from MD runs performed at 300 and 1000 K using set II of FF parameters. Solid lines indicate the average and dashed ones the largest and lowest values. For the highlighted snapshots, the electrostatic potential generated by the solvent mapped over a smoothed van der Waals surface[82] of the solute, including solvent molecules at 2.5 Å from the solute (figures generated with the VMD package[83]).

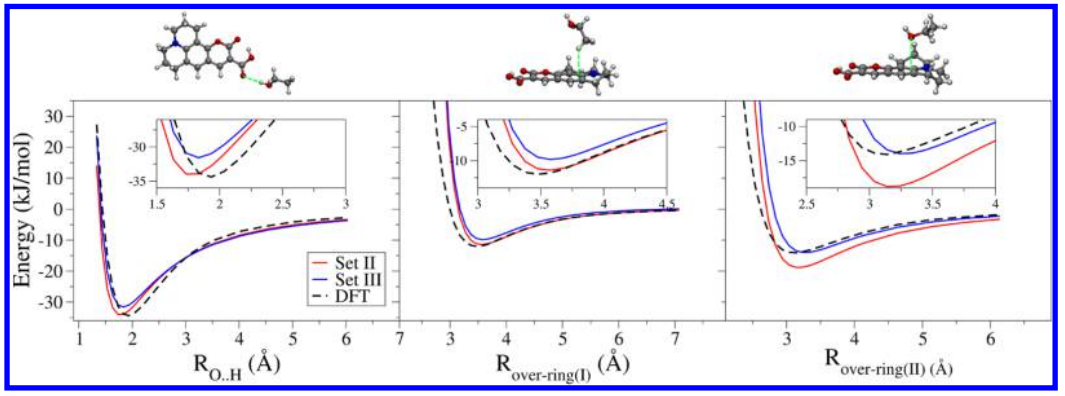

Figure 10. Interaction potential between one ethanol molecule and the coumarin, computed with FF sets II and III and with CAM-B3LYP-D3/6-31G(d) (with counterpoise correction) at different distances along three paths connecting the dye and one solvent molecule (schematic description above the graph). Insets: zoom-in around the potential well.

at different distances from the dye, along the same paths considered in Figure 4. As previously done, we skip set I, as it provides a sampling very similar to set II.

The results are shown in Figure 10. Both FF sets are able to reproduce the hydrogen bond potential curve computed by DFT (although set II better reproduces the well depth). Regarding the description of the solute−solvent interaction as the EtOH molecule approaches the coumarin rings, two distinct situations are considered, with the solvent orienting either the aliphatic (methyl) or polar (hydroxyl) moieties toward the dye. Although the differences are smaller when the solvent faces the methyl group of the coumarin, in both cases the DFT curves increase more smoothly than the FF curves at short distances. Indeed, according to the DFT calculation, the solvent should get closer to the dye when the second and third arrangements are considered. On the same line, when dealing with interaction between the OH group of the solvent and the investigated region of the dye (left and right panels), the QM curve appears to be slightly wider that the ones obtained with the FFs, suggesting larger fluctuations. The analysis of Figures 9 and 10 suggests that refining the MM potentials on the grounds of DFT data would yield a larger solvent distribution and, therefore, a larger broadening, thus correcting, at least partially, the underestimation found with the explicit model here adopted.

The inaccuracies of the FF that lead to the latter underestimation may be traced back to either a lack in the LJ parameters transferability or to the limitations of the scheme

DOI: 10.1021/acs.jctc.5b00870
J. Chem. Theory Comput. 2015, 11, 5810−5825

used for the partial charges. For instance, if polarizable charges are used, it is expected that two molecules can get closer as they become polarized by each other. However, considering the relative weight of the LJ and Coulomb contributions to the intermolecular energy shown in Figure 4, it can be hypothesized that a reliable FF refinement should focus first on the LJ parameters that rule the solute−solvent interaction.

In summary, in this section we analyzed possible causes responsible for an underestimation of solvent broadening, within the model adopted in this paper, i.e., the hypothesis that solvent and solute degrees of freedom can be separated. It is worth reminding, however, that the origin of the underestimation may partially reside as well in the separation of solute−solvent modes and in the frozen solute approximation adopted herein. For example, the interaction with a rigid solute may not allow an accurate description of the properties of the solvation sphere, and the choice to constrain the solvent bond lengths may bias the spontaneous formation of intermolecular H-bonds. For all these reasons, future work will be devoted to further analysis of the problem, and the role of specific H-bonds will be reinvestigated considering also intramolecular flexibility.

6. CONCLUSIONS

This work presents a step in our research line devoted to the establishment of robust computational protocols to combine solute vibrationally resolved line shapes and solvent broadening effects. The ultimate goal is to achieve accurate *in silico* simulations of the absorption spectra of dyes in complex environments without resorting to phenomenological parameters. In this framework, here we check the performance of models that simulate the spectrum from a convolution of separate contributions of the solute and the solvent. More in detail, we propose and test a computational protocol to simulate solvent inhomogeneous broadening based on explicit solvent models and MD simulations to sample solvent fluctuations around the solute, constrained in its GS equilibrium geometry.

The predictions of this approach are compared with those obtained through implicit models, exploiting the Marcus classical expression that connects the broadening with the solvent reorganization energy. While the latter procedure was already successfully adopted in a few cases for which the modeling of specific solute−solvent interactions was not essential,[15,27,38,54] we believe that robust protocols for estimating solvent broadening from explicit solvent models would improve the possibility to accurately simulate environmental broadening effects due to specific interactions or even in complex environments like heterogeneous media.

At variance with traditional approaches based on the classical MD of the solute−solvent supersystem, we adopt MD for the solvent only. This allows for preserving, in a computationally simple way, the separation of solute and solvent, and to undergo a full quantum description of the solute line shape. According to a well-established procedure for semi-rigid molecules, the latter is obtained in harmonic approximation from the vibronic transitions between the initial and final electronic surfaces computed in PCM so as to account for mean-field solvent effects.

The price that is paid in our procedure is inherent in the assumption that is possible to define the spectrum as a convolution of solute and solvent components. As we discussed in section 2, this means to assume that, while both solute and solvent coordinates rearrange after the electronic transition of the solute, their motions can be decoupled. Therefore, instantaneous solute−solvent couplings are neglected and replaced by mean-field effects. Additionally, due to the necessity to resort to harmonic model PES for large solutes, the effect of anharmonicities, approximately captured by MD simulations, is neglected, too.

As far as the solvent inhomogeneous broadening is concerned, the discussion in section 2 highlights that both computational routes, based on either implicit or explicit solvent models, can be derived in the common framework of a classical approximation of the quantum expression for the solvent line shape. The predictions of these two alternative protocols are compared by computing the absorption spectra in EtOH of a series of five structurally related coumarins, recently used for dye-sensitized solar cells.[78−81,86]

Our results show that the explicit models predict solvent broadenings which are systematically narrower than those simulated with the implicit one. The latter, when convoluted with the quantum line shape of the solute, provides simulated spectra that agree better with the experimental observations. Notwithstanding this difference, both implicit and explicit approaches give very similar qualitative trends regarding the change of the solvent contribution for the different dyes, which appear to be connected to different CT characters of their $S_0 \rightarrow S_1$ transition. Even more interestingly, when there are discrepancies in the qualitative trends, e.g., when going from c343 to nkx-2398, or when changing the solvent of c343, the predictions of the explicit model agree better with the relative changes observed experimentally.

Turning to the analysis of the underestimation of the broadening with explicit models, it is noteworthy that practically the same results were obtained by adopting different sets of FF parameters or exploiting different QM/MM partitions to describe the system. These different options provide in fact (slight) changes of the spectrum first moment but not of its variance. Our analysis indicates that at least part of the underestimation of QM/MM solvent broadening arises from an inaccurate sampling of its configuration around the solute. As a matter of fact, we have found that the interactions between the solvent and the coumarin with the adopted empirical FF show inaccuracies for positions close to the dye. Specifically, computations at dispersion-corrected DFT level show that the solvent may get closer to the solute. The adoption of a refined FF able to correct this problem could lead to a larger dispersion of the vertical energies and, according to our analysis, to a larger broadening.

It is not possible to exclude, however, that the origin of the problem partially resides also in the basic assumptions of the adopted model, namely the harmonic approximation of the solute PES and the separation of solute and solvent contributions. In fact, at least the larger dyes of the investigated series should exhibit some flexibility of the conjugated chain that may be coupled with solvent motions and with the electronic transition, leading to broadening effects here neglected. It should be noticed that, since both of these assumptions are made also when the spectrum is obtained with implicit solvent models, this would imply that the good performance in Figure 7 is partially biased by a compensation of errors. Although this may seem unlikely because the SS-PCM protocol provided good estimates of the broadening, even for rather rigid molecules like the smallest coumarin investigated here, c343,[39] coumarin C153 and *N*-methyl-6-Quinolinium betaine in polar aprotic solvents,[15] where flexibility and specific

DOI: 10.1021/acs.jctc.5b00870
J. Chem. Theory Comput. 2015, 11, 5810−5825

solute−solvent interactions are not expected to be important, we think that is worth investigating further this possibility, and that will be done in future works. From a different perspective, the problem when using explicit solvent models could be rooted in the practical method (the MD around a frozen solute) through which we force the decoupling between solute and solvent degrees of freedom, since this may also introduce more subtle biases than those described above. We refer to the fact that it is possible that the microsolvation itself around the solute cannot be accurately described with an explicit solvent model if the solute is completely rigid, since this may lead to artifacts altering the lifetimes of some specific interactions and favoring/disfavoring some interactions with respect to the others. Such artifacts may therefore generate a partially unbalanced sampling and cause, indirectly, an inaccuracy in the estimate of the broadening. Although alternative routes have been proposed in the literature to define a pure solvent contribution to the solvent shape (see, e.g., ref 23), the definition of solvent broadening adopted in this work has the benefit to be directly associated with the hypothesis of the separation of the modes made in section 2, and this leads straightforwardly to a working expression of the total spectrum as a convolution of the solute and solvent contributions. Deriving an equivalent expression with alternative definitions of the solvent broadening would be less immediate.

In summary, the present work represents an intermediate step toward a full understanding of the relative role of different factors in determining the spectral width of dyes in solution. Further insight could come from the development of novel models able to combine quantum (vibronic) solute spectra and solvent contributions without enforcing the decoupling of their motions. This is the challenge for the near future, and a few groups are moving in this direction.[21,25,27,40,87]

As a concluding remark, it is worth noticing that, despite the discussed inaccuracies, the adoption of explicit solvent models in this contribution has allowed us to obtain a detailed microscopic picture of solvent broadening, suggesting that it is not dominated by specific and directional interactions like H-bonds; in fact, different FF predicting different strength for H-bonds provide quite similar estimates for the broadening. On the contrary, the analysis of the electrostatic potential induced by the solvent on the solute indicates that the broadening is mainly connected with the occurrence of solvent configurations that stabilize/destabilize the charge displacement from the amino region to the conjugated ring triggered by the electronic transition.

■ ASSOCIATED CONTENT

Supporting Information

The Supporting Information is available free of charge on the ACS Publications website at DOI: 10.1021/acs.jctc.5b00870.

Additional analysis on c343: description of HOMO−LUMO orbitals and difference density; point charges computed with RESP(HF), RESP(CAM), and CM5-(CAM) methods; RDF plots describing O(coumarin)−EtOH pairs and spatial distribution functions for hydroxyl atoms in EtOH; preliminary tests to set the QM/MM model system; distribution of E_V with different basis sets and using PCM; additional snapshots showing the electrostatic potential generated by the solvent; high-resolution vibronic spectra of all dyes; benchmark calculations on DFT-D3 interaction energies, including Figures S1−S11 and Tables S1−S6 (PDF)

■ AUTHOR INFORMATION

Corresponding Author

*E-mail: fabrizio.santoro@iccom.cnr.it.

Notes

The authors declare no competing financial interest.

■ ACKNOWLEDGMENTS

The support of MIUR (PRIN 2010-2011 prot. 2010ERFKXL) and of the Italian Institute of Technology (IIT-Seed HELYOS) is acknowledged. J.C. acknowledges "Fundación Ramón Areces" for funding his postdoctoral position, and the Pisa Unit of ICCOM-CNR Pisa for hospitality. F.J.A.F. acknowledges support from the Marie Curie COFUND programme U-Mobility, co-financed by the University of Malaga, the European Commission FP7 under GA No. 246550, and Ministerio de Economía y Competitividad (COFUND2013-40259).

■ REFERENCES

(1) Hazra, A.; Nooijen, M. Derivation and Efficient Implementation of a Recursion Formula to Calculate Harmonic Franck-Condon Factors for Polyatomic Molecules. *Int. J. Quantum Chem.* **2003**, *95*, 643−657.

(2) Dierksen, M.; Grimme, S. An Efficient Approach for the Calculation of Franck-Condon Integrals of Large Molecules. *J. Chem. Phys.* **2005**, *122*, 244101.

(3) Santoro, F.; Lami, A.; Improta, R.; Barone, V. Effective method to compute vibrationally resolved optical spectra of large molecules at finite temperature in the gas phase and in solution. *J. Chem. Phys.* **2007**, *126*, 184102.

(4) (a) Santoro, F.; Improta, R.; Lami, A.; Bloino, J.; Barone, V. Effective method to compute Franck-Condon integrals for optical spectra of large molecules in solution. *J. Chem. Phys.* **2007**, *126*, 084509. (b) Santoro, F.; Improta, R.; Lami, A.; Bloino, J.; Barone, V. Erratum: "Effective method to compute Franck-Condon integrals for optical spectra of large molecules in solution" [J. Chem. Phys.126, 084509 (2007)]. *J. Chem. Phys.* **2007**, *126*, 169903.

(5) Santoro, F.; Lami, A.; Improta, R.; Bloino, J.; Barone, V. Effective method for the computation of optical spectra of large molecules at finite temperature including the Duschinsky and Herzberg-Teller effect: The Qx band of porphyrin as a case study. *J. Chem. Phys.* **2008**, *128*, 224311.

(6) Jankowiak, H.-C.; Stuber, J. L.; Berger, R. Vibronic Transitions in Large Molecular Systems: Rigorous Prescreening Conditions for Franck-Condon Factors. *J. Chem. Phys.* **2007**, *127*, 234101.

(7) Bloino, J.; Biczysko, M.; Santoro, F.; Barone, V. General Approach to Compute Vibrationally Resolved One-Photon Electronic Spectra. *J. Chem. Theory Comput.* **2010**, *6*, 1256−1274.

(8) Tang, J.; Lee, M. T.; Lin, S. H. Effects of the Duschinsky mode-mixing mechanism on temperature dependence of electron transfer processes. *J. Chem. Phys.* **2003**, *119*, 7188−7196.

(9) Ianconescu, R.; Pollak, E. Photoinduced Cooling of Polyatomic Molecules in an Electronically Excited State in the Presence of Dushinskii Rotations. *J. Phys. Chem. A* **2004**, *108*, 7778−7784.

(10) Peng, Q.; Niu, Y.; Deng, C.; Shuai, Z. Vibration correlation function formalism of radiative and non-radiative rates for complex molecules. *Chem. Phys.* **2010**, *370*, 215−222.

(11) Lami, A.; Santoro, F. In *Computational Strategies for Spectroscopy*; Barone, V., Ed.; John Wiley & Sons, Inc.: New York, 2011; Chapter 10, pp 475−516.

(12) Huh, J.; Berger, R. Coherent state-based generating function approach for Franck-Condon transitions and beyond. *J. Phys.: Conf. Ser.* **2012**, *380*, 012019.

DOI: 10.1021/acs.jctc.5b00870
J. Chem. Theory Comput. 2015, 11, 5810−5825

(13) Borrelli, R.; Capobianco, A.; Peluso, A. Generating Function Approach to the Calculation of Spectral Band Shapes of Free-Base Chlorin Including Duschinsky and Herzberg-Teller Effects. *J. Phys. Chem. A* **2012**, *116*, 9934−9940.
(14) Baiardi, A.; Bloino, J.; Barone, V. General Time Dependent Approach to Vibronic Spectroscopy Including Franck-Condon, Herzberg-Teller, and Duschinsky Effects. *J. Chem. Theory Comput.* **2013**, *9*, 4097−4115.
(15) Avila Ferrer, F. J.; Cerezo, J.; Soto, J.; Improta, R.; Santoro, F. First-principle computation of absorption and fluorescence spectra in solution accounting for vibronic structure, temperature effects and solvent inhomogenous broadening. *Comput. Theor. Chem.* **2014**, *1040−1041*, 328−337.
(16) Etinski, M.; Rai-Constapel, V.; Marian, C. M. Time-dependent approach to spin-vibronic coupling: Implementation and assessment. *J. Chem. Phys.* **2014**, *140*, 114104.
(17) Barone, V.; Bloino, J.; Monti, S.; Pedone, A.; Prampolini, G. Theoretical multilevel approach for studying the photophysical properties of organic dyes in solution. *Phys. Chem. Chem. Phys.* **2010**, *12*, 10550−10561.
(18) De Mitri, N.; Monti, S.; Prampolini, G.; Barone, V. Absorption and Emission Spectra of a Flexible Dye in Solution: A Computational Time-Dependent Approach. *J. Chem. Theory Comput.* **2013**, *9*, 4507−4516.
(19) Cacelli, I.; Ferretti, A.; Prampolini, G. Perturbative Multireference Configuration Interaction (CI-MRPT2) Calculations in a Focused Dynamical Approach: A Computational Study of Solvatochromism in Pyrimidine. *J. Phys. Chem. A* **2015**, *119*, 5250−5259.
(20) Eilmes, A. Effect of Molecular Vibrations on the MD/QC-Simulated Absorption Spectra. *Int. J. Quantum Chem.* **2014**, *114*, 261−270.
(21) Zalenśy, R.; Murugan, N. A.; Gelmukhanov, F.; Rinkevicius, Z.; Ośmialowski, B.; Bartkowiak, W.; Ågren, H. Toward Fully Nonempirical Simulations of Optical Band Shapes of Molecules in Solution: a Case Study of Heterocyclic Ketoimine Difluoroborates. *J. Phys. Chem. A* **2015**, *119*, 5145−5152.
(22) Petrone, A.; Donati, G.; Caruso, P.; Rega, N. Understanding THZ and IR Signals Beneath Time-Resolved Fluorescence from Excited-State Ab Initio Dynamics. *J. Am. Chem. Soc.* **2014**, *136*, 14866−14874.
(23) Petrone, A.; Cerezo, J.; Ferrer, F. J. A.; Donati, G.; Improta, R.; Rega, N.; Santoro, F. Absorption and Emission Spectral Shapes of a Prototype Dye in Water by Combining Classical/Dynamical and Quantum/Static Approaches. *J. Phys. Chem. A* **2015**, *119*, 5426−5438.
(24) D'Alessandro, M.; Aschi, M.; Mazzuca, C.; Palleschi, A.; Amadei, A. Theoretical modeling of UV-Vis absorption and emission spectra in liquid state systems including vibrational and conformational effects: The vertical transition approximation. *J. Chem. Phys.* **2013**, *139*, 114102.
(25) D'Abramo, M.; Aschi, M.; Amadei, A. Theoretical modeling of UV-Vis absorption and emission spectra in liquid state systems including vibrational and conformational effects: Explicit treatment of the vibronic transitions. *J. Chem. Phys.* **2014**, *140*, 164104.
(26) Arul Murugan, N.; Kongsted, J.; Rinkevicius, Z.; Aidas, K.; Mikkelsen, K. V.; Agren, H. Hybrid density functional theory/molecular mechanics calculations of two-photon absorption of dimethylamino nitro stilbene in solution. *Phys. Chem. Chem. Phys.* **2011**, *13*, 12506−12516.
(27) Benassi, E.; Cappelli, C.; Carlotti, B.; Barone, V. An integrated computational tool to model the broadening of the absorption bands of flexible dyes in solution: Cationic chromophores as test cases. *Phys. Chem. Chem. Phys.* **2014**, *16*, 26963−26973.
(28) Lax, M. The Franck-Condon Principle and Its Application to Crystals. *J. Chem. Phys.* **1952**, *20*, 1752−1760.
(29) Biczysko, M.; Bloino, J.; Santoro, F.; Barone, V. In *Computational Strategies for Spectroscopy: from Small Molecules to Nanosystems*; Barone, V., Ed.; John Wiley & Sons, Inc.: New York, 2011; Chapter 8, pp 361−443.
(30) Horng, M. L.; Gardecki, J. A.; Papazyan, A.; Maroncelli, M. Subpicosecond Measurements of Polar Solvation Dynamics: Coumarin 153 Revisited. *J. Phys. Chem.* **1995**, *99*, 17311−17337.
(31) Karunakaran, V.; Senyushkina, T.; Saroja, G.; Ernsting, N. P.; Liebscher, J. 2-Amino-7-nitro-fluorenes in Neat and Mixed Solvents s Optical Band Shapes and Solvatochromism. *J. Phys. Chem. A* **2007**, *111*, 10944−10952.
(32) Tomasi, J.; Mennucci, B.; Cammi, R. Quantum Mechanical Continuum Solvation Models. *Chem. Rev.* **2005**, *105*, 2999−3094.
(33) Improta, R.; Barone, V.; Santoro, F. Ab Initio Calculations of Absorption Spectra of Large Molecules in Solution: Coumarin C153. *Angew. Chem., Int. Ed.* **2007**, *46*, 405−408.
(34) Mennucci, B.; Cappelli, C.; Guido, C. A.; Cammi, R.; Tomasi, J. Structures and Properties of Electronically Excited Chromophores in Solution from the Polarizable Continuum Model Coupled to the Time-Dependent Density Functional Theory. *J. Phys. Chem. A* **2009**, *113*, 3009−3020.
(35) Jacquemin, D.; Brémond, E.; Planchat, A.; Ciofini, I.; Adamo, C. TD-DFT Vibronic Couplings in Anthraquinones: From Basis Set and Functional Benchmarks to Applications for Industrial Dyes. *J. Chem. Theory Comput.* **2011**, *7*, 1882−1892.
(36) Barone, V.; Biczysko, M.; Bloino, J.; Carta, L.; Pedone, A. Environmental and dynamical effects on the optical properties of molecular systems by time-independent and time-dependent approaches: Coumarin derivatives as test cases. *Comput. Theor. Chem.* **2014**, *1037*, 35−48.
(37) Marcus, R. A. Relation between charge transfer absorption and fluorescence spectra and the inverted region. *J. Phys. Chem.* **1989**, *93*, 3078−3086.
(38) Avila Ferrer, F. J.; Improta, R.; Santoro, F.; Barone, V. Computing the inhomogeneous broadening of electronic transitions in solution: a first-principle quantum mechanical approach. *Phys. Chem. Chem. Phys.* **2011**, *13*, 17007−17012.
(39) Cerezo, J.; Avila Ferrer, F. J.; Santoro, F. Disentangling vibronic and solvent broadening effects in the absorption spectra of coumarin derivatives for dyes sensitized solar cells. *Phys. Chem. Chem. Phys.* **2015**, *17*, 11401−11411.
(40) Avila Ferrer, F. J.; Davari, M. D.; Morozov, D.; Groenhof, G.; Santoro, F. The Lineshape of the Electronic Spectrum of the Green Fluorescent Protein Chromophore, Part II: Solution Phase. *ChemPhysChem* **2014**, *15*, 3246−3257.
(41) Tatchen, J.; Pollak, E. Ab initio spectroscopy and photoinduced cooling of the trans-stilbene molecule. *J. Chem. Phys.* **2008**, *128*, 164303.
(42) Mukamel, S. *Principles of Nonlinear Optical Spectroscopy*; Oxford University Press: New York, 1995.
(43) Bergsma, J. P.; Berens, P. H.; Wilson, K. R.; Fredkin, D. R.; Heller, E. J. Electronic spectra from molecular dynamics: a simple approach. *J. Phys. Chem.* **1984**, *88*, 612−619.
(44) Tannor, D. J. *Introduction to Quantum Mechanics: a Time-Dependent Perspective*; University Science Books: Sausalito, CA, 2007.
(45) Kestner, N. R.; Logan, J.; Jortner, J. Thermal electron transfer reactions in polar solvents. *J. Phys. Chem.* **1974**, *78*, 2148−2166.
(46) Weiss, U. *Quantum Dissipative Systems*; World Scientific Publishing Co.: Singapore, 1993.
(47) Markham, J. J. Interaction of Normal Modes with Electron Traps. *Rev. Mod. Phys.* **1959**, *31*, 956−989.
(48) Marcus, R. A. Interactions in Polar Media. I. Interparticle Interaction Energy. *J. Chem. Phys.* **1963**, *38*, 1335−1340.
(49) Marcus, R. A. Interactions in Polar Media. II. Continua. *J. Chem. Phys.* **1963**, *39*, 460−469.
(50) Marcus, R. A. Free Energy of Nonequilibrium Polarization Systems. III. Statistical Mechanics of Homogeneous and Electrode Systems. *J. Chem. Phys.* **1963**, *39*, 1734−1740.
(51) Cammi, R.; Corni, S.; Mennucci, B.; Tomasi, J. Electronic excitation energies of molecules in solution: State specific and linear response methods for nonequilibrium continuum solvation models. *J. Chem. Phys.* **2005**, *122*, 104513.

DOI: 10.1021/acs.jctc.5b00870
J. Chem. Theory Comput. 2015, 11, 5810−5825

(52) (a) Corni, S.; Cammi, R.; Mennucci, B.; Tomasi, J. Electronic excitation energies of molecules in solution within continuum solvation models: Investigating the discrepancy between state-specific and linear-response methods. *J. Chem. Phys.* **2005**, *123*, 134512. (b) Caricato, M.; Mennucci, B.; Tomasi, J.; Ingrosso, F.; Cammi, R.; Corni, S.; Scalmani, G. Formation and relaxation of excited states in solution: A new time dependent polarizable continuum model based on time dependent density functional theory. *J. Chem. Phys.* **2006**, *124*, 124520.
(53) Improta, R.; Scalmani, G.; Frisch, M. J.; Barone, V. Toward effective and reliable fluorescence energies in solution by a new state specific polarizable continuum model time dependent density functional theory approach. *J. Chem. Phys.* **2007**, *127*, 074504.
(54) Lapini, A.; Fabbrizzi, P.; Piccardo, M.; di Donato, M.; Lascialfari, L.; Foggi, P.; Cicchi, S.; Biczysko, M.; Carnimeo, I.; Santoro, F.; Cappelli, C.; Righini, R. Ultrafast resonance energy transfer in the umbelliferone-alizarin bichromophore. *Phys. Chem. Chem. Phys.* **2014**, *16*, 10059−10074.
(55) Pronk, S.; Páll, S.; Schulz, R.; Larsson, P.; Bjelkmar, P.; Apostolov, R.; Shirts, M. R.; Smith, J. C.; Kasson, P. M.; van der Spoel, D.; Hess, B.; Lindahl, E. GROMACS 4.5: a high-throughput and highly parallel open source molecular simulation toolkit. *Bioinformatics* **2013**, *29*, 845−854.
(56) Wang, J.; Wolf, R. M.; Caldwell, J. W.; Kollman, P. A.; Case, D. A. Development and testing of a general amber force field. *J. Comput. Chem.* **2004**, *25*, 1157−1174.
(57) Jorgensen, W. L.; Maxwell, D. S.; Tirado-Rives, J. Development and Testing of the OPLS All-Atom Force Field on Conformational Energetics and Properties of Organic Liquids. *J. Am. Chem. Soc.* **1996**, *118*, 11225−11236.
(58) Caleman, C.; van Maaren, P. J.; Hong, M.; Hub, J. S.; Costa, L. T.; van der Spoel, D. Force Field Benchmark of Organic Liquids: Density, Enthalpy of Vaporization, Heat Capacities, Surface Tension, Isothermal Compressibility, Volumetric Expansion Coefficient, and Dielectric Constant. *J. Chem. Theory Comput.* **2012**, *8*, 61−74.
(59) Wang, J.; Cieplak, P.; Kollman, P. A. How well does a restrained electrostatic potential (RESP) model perform in calculating conformational energies of organic and biological molecules? *J. Comput. Chem.* **2000**, *21*, 1049−1074.
(60) Marenich, A. V.; Jerome, S. V.; Cramer, C. J.; Truhlar, D. G. Charge Model 5: An Extension of Hirshfeld Population Analysis for the Accurate Description of Molecular Interactions in Gaseous and Condensed Phases. *J. Chem. Theory Comput.* **2012**, *8*, 527−541.
(61) Darden, T.; York, D.; Pedersen, L. Particle mesh Ewald: An N-log(N) method for Ewald sums in large systems. *J. Chem. Phys.* **1993**, *98*, 10089−10092.
(62) Berendsen, H. J. C.; Postma, J. P. M.; van Gunsteren, W. F.; DiNola, A.; Haak, J. R. Molecular dynamics with coupling to an external bath. *J. Chem. Phys.* **1984**, *81*, 3684−3690.
(63) Hoover, W. G. Canonical dynamics: Equilibrium phase-space distributions. *Phys. Rev. A: At., Mol., Opt. Phys.* **1985**, *31*, 1695−1697.
(64) Hess, B.; Bekker, H.; Berendsen, H. J. C.; Fraaije, J. G. E. M. LINCS: a linear constraint solver for molecular simulations. *J. Comput. Chem.* **1997**, *18*, 1463−1472.
(65) Yanai, T.; Tew, D. P.; Handy, N. C. A new hybrid exchange-correlation functional using the Coulomb-attenuating method (CAM-B3LYP). *Chem. Phys. Lett.* **2004**, *393*, 51−57.
(66) Frisch, M. J.; Trucks, G. W.; Schlegel, H. B.; Scuseria, G. E.; Robb, M. A.; Cheeseman, J. R.; Scalmani, G.; Barone, V.; Mennucci, B.; Petersson, G. A.; Nakatsuji, H.; Caricato, M.; Li, X.; Hratchian, H. P.; Izmaylov, A. F.; Bloino, J.; Zheng, G.; Sonnenberg, J. L.; Hada, M.; Ehara, M.; Toyota, K.; Fukuda, R.; Hasegawa, J.; Ishida, M.; Nakajima, T.; Honda, Y.; Kitao, O.; Nakai, H.; Vreven, T.; Montgomery, J. A., Jr.; Peralta, J. E.; Ogliaro, F.; Bearpark, M.; Heyd, J. J.; Brothers, E.; Kudin, K. N.; Staroverov, V. N.; Kobayashi, R.; Normand, J.; Raghavachari, K.; Rendell, A.; Burant, J. C.; Iyengar, S. S.; Tomasi, J.; Cossi, M.; Rega, N.; Millam, J. M.; Klene, M.; Knox, J. E.; Cross, J. B.; Bakken, V.; Adamo, C.; Jaramillo, J.; Gomperts, R.; Stratmann, R. E.; Yazyev, O.; Austin, A. J.; Cammi, R.; Pomelli, C.; Ochterski, J. W.; Martin, R. L.; Morokuma, K.; Zakrzewski, V. G.; Voth, G. A.; Salvador, P.; Dannenberg, J. J.; Dapprich, S.; Daniels, A. D.; Farkas, O.; Foresman, J. B.; Ortiz, J. V.; Cioslowski, J.; Fox, D. J. *Gaussian 09*, Revision A.2; Gaussian Inc.: Wallingford CT, 2009.
(67) Charaf-Eddin, A.; Planchat, A.; Mennucci, B.; Adamo, C.; Jacquemin, D. Choosing a Functional for Computing Absorption and Fluorescence Band Shapes with TD-DFT. *J. Chem. Theory Comput.* **2013**, *9*, 2749−2760.
(68) Avila Ferrer, F. J.; Santoro, F. Comparison of vertical and adiabatic harmonic approaches for the calculation of the vibrational structure of electronic spectra. *Phys. Chem. Chem. Phys.* **2012**, *14*, 13549−13563.
(69) Duschinsky, F. On the Interpretation of Electronic Spectra of Polyatomic Molecules. I. The Franck-Condon Principle. *Acta Physicochim.: URSS* **1937**, *7*, 551−566.
(70) Cerezo, J.; Zúñiga, J.; Requena, A.; Ávila Ferrer, F. J.; Santoro, F. Harmonic Models in Cartesian and Internal Coordinates to Simulate the Absorption Spectra of Carotenoids at Finite Temperatures. *J. Chem. Theory Comput.* **2013**, *9*, 4947−4958.
(71) Cerezo, J.; Zúñiga, J.; Requena, A.; Ávila Ferrer, F. J.; Santoro, F. Erratum: Harmonic Models in Cartesian and Internal Coordinates to Simulate the Absorption Spectra of Carotenoids at Finite Temperatures. *J. Chem. Theory Comput.* **2014**, *10*, 3586−3587.
(72) Improta, R. *Computational Strategies for Spectroscopy*; John Wiley & Sons, Inc.: New York, 2011; pp 37−75.
(73) Santoro, F. *FCclasses*, a Fortran 77 code, development version. The standard version of the code can be downloaded at http://www.pi.iccom.cnr.it/fcclasses, last accessed Nov 2, 2015. To use the development version, necessary to run TD calculations (see ref 74), please contact the author.
(74) Cerezo, J.; Santoro, F. *TDspectrum*, a routine for TD calculations within FCclasses, 2013.
(75) Isborn, C. M.; Mar, B. D.; Curchod, B. F. E.; Tavernelli, I.; Martínez, T. J. The Charge Transfer Problem in Density Functional Theory Calculations of Aqueously Solvated Molecules. *J. Phys. Chem. B* **2013**, *117*, 12189−12201.
(76) Correa, N. M.; Levinger, N. E. What can you learn from a molecular probe? New insights on the behavior of C343 in homogeneous solutions and AOT reverse micelles. *J. Phys. Chem. B* **2006**, *110*, 13050−13061.
(77) Liu, X.; Cole, J. M.; Low, K. S. Molecular Origins of Dye Aggregation and Complex Formation Effects in Coumarin 343. *J. Phys. Chem. C* **2013**, *117*, 14723−14730.
(78) Hara, K.; Sayama, K.; Ohga, Y.; Shinpo, A.; Suga, S.; Arakawa, H. A coumarin-derivative dye sensitized nanocrystalline TiO solar cell having a high solar-energy conversion efficiency up to 5.6%. *Chem. Commun.* **2001**, 569−570.
(79) Hara, K.; Sato, T.; Katoh, R.; Furube, A.; Ohga, Y.; Shinpo, A.; Suga, S.; Sayama, K.; Sugihara, H.; Arakawa, H. Molecular Design of Coumarin Dyes for Efficient Dye-Sensitized Solar Cells. *J. Phys. Chem. B* **2003**, *107*, 597−606.
(80) Hara, K.; Tachibana, Y.; Ohga, Y.; Shinpo, A.; Suga, S.; Sayama, K.; Sugihara, H.; Arakawa, H. Dye-sensitized nanocrystalline TiO2 solar cells based on novel coumarin dyes. *Sol. Energy Mater. Sol. Cells* **2003**, *77*, 89−103.
(81) Wang, Z.-S.; Hara, K.; Dan-oh, Y.; Kasada, C.; Shinpo, A.; Suga, S.; Arakawa, H.; Sugihara, H. Photophysical and (Photo)-electrochemical Properties of a Coumarin Dye. *J. Phys. Chem. B* **2005**, *109*, 3907−3914.
(82) Varshney, A.; Brooks, F. P.; Wright, W. V. Linearly Scalable Computation of Smooth Molecular Surfaces. *IEEE. Comput. Graph.* **1994**, *14*, 19−25.
(83) Humphrey, W.; Dalke, A.; Schulten, K. VMD - Visual Molecular Dynamics. *J. Mol. Graphics* **1996**, *14*, 33−38.
(84) Grimme, S.; Antony, J.; Ehrlich, S.; Krieg, H. A consistent and accurate ab initio parametrization of density functional dispersion correction (DFT-D) for the 94 elements H-Pu. *J. Chem. Phys.* **2010**, *132*, 154104.

DOI: 10.1021/acs.jctc.5b00870
J. Chem. Theory Comput. 2015, 11, 5810−5825

(85) Goerigk, L.; Grimme, S. A thorough benchmark of density functional methods for general main group thermochemistry, kinetics, and noncovalent interactions. *Phys. Chem. Chem. Phys.* **2011**, *13*, 6670−6688.
(86) Pant, D.; Le Guennec, M.; Illien, B.; Girault, H. H. The pH dependent adsorption of Coumarin 343 at the water/dichloroethane interface. *Phys. Chem. Chem. Phys.* **2004**, *6*, 3140−3146.
(87) Improta, R.; Ferrer, F. J. A.; Stendardo, E.; Santoro, F. Quantum-Classical Calculation of the Absorption and Emission Spectral Shapes of Oligothiophenes at Low and Room Temperature by First-Principle Calculations. *ChemPhysChem* **2014**, *15*, 3320−3333.

DOI: 10.1021/acs.jctc.5b00870
J. Chem. Theory Comput. 2015, 11, 5810−5825